Predicting Flight by Flight Fatigue Crack Growth Rates

J. P. Gallagher* and H. D. Stalnaker†
Air Force Flight Dynamics Laboratory, Wright-Patterson Air Force Base, Ohio

Several crack growth prediction approaches are examined for their ability to predict both the magnitude and trend of fatigue crack growth rate data generated under transport wing flight simulation loading. Three cycle-by-cycle accounting approaches, one with no load interaction and two which incorporate high-to-low load interaction, are studied. Two stress-stress intensity factor characterization approaches are also examined. These two characterization approaches isolate principal variables from the input stress spectrum and then utilize the no-load interaction, cycle-by-cycle approach to obtain estimates of crack growth rates. The results indicate that load interaction cycle-by-cycle accounting procedures lead to more accurate crack growth predictions principally because they incorporate the influence of the high-to-low load interaction phenemonon.

Nomenclature

a	= crack length
da/dN	= cyclic crack growth rate based on constant amplitude loading
da/dF	= average growth rate for a typical flight
C, p	= growth rate constants
F	= flight
K	= stress intensity factor
K_R	= residual stress intensity factor
K_{th}	= maximum stress intensity factor at the threshold level of fatigue cracking
N	= cycle count
N_F	= number of cycles in any flight
N_{50}	= number of cycles in any group of 50 flights
R	= stress ratio
S	= overload shut-off ratio, establishing a condition of no-fatigue crack growth following an overload
Z^{OL}	= overload created load interaction zone
γ	= parameter relating yield zone radius to Z^{OL}
Δa	= incremental crack movement defined by a block of 50 flights
Δa^{OL}	= incremental crack movement generated by low loads applied subsequent to high load, measured from crack position defined by high-load cycle
ΔK	= range of stress intensity
$\Delta\sigma$	= range of stress
σ	= stress
σ_{ys}	= yield strength

Superscripts and Subscripts

eff	= effective
OL	= associated with overload
p	= peak
W	= Willenborg
∞	= associated with remote loads
avg	= average
f	= final
F	= flight
max	= maximum
min	= minimum
o	= initial
—	= bar over parameter indicates rms function

Presented as Paper 74-367 at the AIAA/ASME/SAE/5th Structures, Structural Dynamics and Materials Conference, Las Vegas, Nevada, April 17-19, 1974; submitted May 7, 1974; revision received January 20, 1975. The authors wish to express their sincere appreciation to R. L. Cavanagh, J. H. Anderson, F. E. Hussong, H. F. Ostrowski, and I. D. Hearne for collectively making it possible to carry out the experimental program.

Index category: Aircraft Structural Design (including Loads).

*Aerospace Engineer, Structural Integrity Branch.

†Aerospace Engineer, Experimental Branch.

Introduction

TWO general methods have been proposed for predicting fatigue crack growth behavior of spectrum loaded structures. One method utilizes cycle-by-cycle accounting procedures to determine the advance of a crack for each applied load cycle.[1-6] The other method characterizes the spectrum with significant root mean square (rms) load variables prior to predicting the average crack movement expected per cycle at a given crack length.[7-11]

Brussat[1] employed a linear-summation, no-load interaction cycle-by-cycle crack growth predictive approach which accounted for the influence of the stress ratio (R) of each load cycle in the spectra. He found that the predictions were conservative, but normally by less than a factor of two with respect to the spectra generated crack growth rates. Wheeler[2] and Willenborg et al.,[3] suggested two cycle-by-cycle procedures which incorporate high-to-low load interaction effects via crack growth retardation models. Retardation models predict that crack growth rates for low loads applied subsequent to a high load will be significantly slower than if the high load were not applied. Most of the predictions developed using retardation models correlate reasonably well with the spectrum generated crack growth data but both models have deficiencies.[5] Recently, Gallagher and Hughes[12] generalized the Willenborg et al. model so that many of the noted deficiencies[5] were removed.

Paris[7] first suggested that since the stress range has the most pronounced influence on constant amplitude induced crack growth rates, it should be isolated as the most significant parameter in a stress spectrum. Smith,[8,9] Swanson et al.,[10] and Barsom[11] have applied the stress range characterization approach with good success in correlating crack growth rate data generated by random loadings. In the random loadings studied,[7-11] the stress ranges were shown to be closely described by a continuous unimodal distribution stress function; specifically, a Rayleigh distribution function. All investigators[7-11] made clear that the application of the stress characterization approach should be restricted to stress histories which can be described using a continuous unimodal distribution function. The restriction applies principally with respect to stress ranges and secondly to maximum stresses.

The objective of this paper is to evaluate several approaches for characterizing crack growth rate behavior generated under typical transport-wing flight-simulation loading. To achieve this objective, the accuracy of several cycle by cycle crack growth accounting procedures and stress—stress intensity factor characterization approaches are examined on the basis of their ability to predict both the magnitude and trends of crack

growth rate data generated under flight simulation loading. A radial corner crack configuration which is frequently noted to appear in cracked aircraft hardware was chosen to generate the flight-simulation crack growth-rate data. This increased complexity was added only to show the versatility of the analysis procedure.

The cycle-by-cycle crack growth predictive approaches that are examined in this investigation use the load accounting methods identified by Brussat,[1] Willenborg et al.,[3] and Gallagher and Hughes.[12] Barsom's root mean square (rms) stress approach[11] is utilized to characterize the stress range, the maximum stress, and the once per flight peak (min) to peak (max) stress histories.

Spectra

Description of Stress Spectra

Two transport-wing flight-simulation stress histories were employed in this investigation for the generation of crack growth rate data. Spectrum A is representative of the stresses experienced on the upper skin of a transport wing while spectrum B characterizes the stresses experienced by the lower wing skin at a point directly below the upper surface point for which spectrum A applies. Both spectra contained fourteen different types of flights, each representative of a specific mission usage. In general, the flights were composed of one ground to air stress cycle (GTAC) and the taxiing (Spectrum A) or gust/maneuver (Sepctrum B) stresses were arranged in a low-high-low sequence as indicated by Fig. 1. The ordering of the individual mission usage flights was randomized over a sufficiently large block of flights so that the random mission mix block of flights contained a representative fraction of the total number of missions in the expected lifetime (6000 flights) of the aircraft. There were 100 flights in the random mission mix block developed for Spectrum A, and 300 flights for Spectrum B. See Ref. 13 for additional details.

RMS Stress Parameters

In using the root mean square (rms) stress range parameter approach, only the rising (to higher tension) portion of the stress cycle was considered. The reason for choosing the rising stress range approach was suggested by the careful fatigue and fractographic investigation conducted by McMillan and Pelloux[14] and by Barsom's investigation[15] of the influence of wave form on corrosion fatigue crack growth rates. Both investigations identify the rising stress change with fatigue crack movement.

The rms parameter ($\overline{\Delta\sigma}$) used to characterize the combined influence of all positive stress ranges ($\Delta\sigma_i$) in a spectrum containing N cycles was obtained from

$$\overline{\Delta\sigma} = \sum_{i=1}^{N} \left[(\Delta\sigma_i)^2/N \right]^{1/2} \tag{1}$$

Because of the noted influence of stress ratio on constant amplitude fatigue crack growth behavior,[16,17] an rms parameter

$$\overline{\sigma}_{\max} = \sum_{i=1}^{N} \left[(\sigma_{\max_i})^2/N \right]^{1/2} \tag{2}$$

was selected to characterize the maximum stresses A measure of the stress ratio predominating in a spectrum can then be obtained from

$$\bar{R} = 1 - \overline{\Delta\sigma}/\overline{\sigma}_{\max} \tag{3}$$

Listed in Table 1 are the representative rms parameters used to characterize Spectra A (upper surface) and B (lower surface). Also included in Table 1 is the average number of cycles per flight of loading. A second set of representative rms parameters which isolate the once per flight peak (minimum and maximum) stresses are provided in Table 2. These rms peak stress parameters were calculated using an equation similar to Eq. (2).

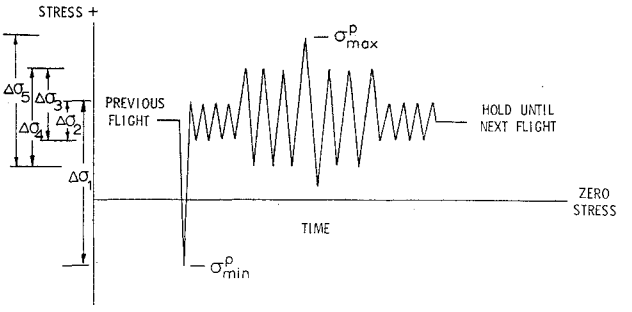

Fig. 1 Flight loading described schematically.

Table 1 Representative rms stress parameters for a given flight

Spectrum	$\overline{\sigma}_{\max}$ (ksi)	$\overline{\Delta\sigma}$ (ksi)	$\bar{R}$	N_F Cycles/flight
A	11.72	6.10	0.480	32
B	12.30	4.45	0.640	351

Table 2 Peak-to-peak stress characterization for a given flight

Spectrum	$\overline{\sigma}^P_{\max}$ (ksi)	$\overline{\sigma}^P_{\min}$ (ksi)	$\bar{R}$	Cycles/flight
A	13.5	−15.2	−1.12	1
B	18.5	−15.1	−0.82	1

Material, Geometry, and Test Methods

Material and Specimen Geometry

Specimens of the type shown in Fig. 2 were machined from extruded (7075-T6511 aluminum alloy) wing stock material. The specimen thickness was 0.250 in. in the gage section. Constant-amplitude and flight-simulation crack growth was monitored for small radial corner flaws growing from 0.250 in. diameter holes. Contained in Table 3 is a listing of initial and final crack-length conditions with the corresponding number of flights elapsed in each spectrum studied. Additional constant amplitude loadings were applied to center cracked panels having the geometry shown in Fig. 2. A single crack was located in each 12-in. bay of the specimen for these constant amplitude tests.

Stress Intensity Factor Coefficient

The Hsu and Liu[18] analysis for a radial corner crack located at the edge of a hole was modified to account for the continuous crack shape changes which were noted to occur during crack growth. The small corner flaws were approximately quarter circular in shape but grew more rapidly along the hole so that when the surface crack length was 0.125 in. the crack along the hole was just reaching through to the

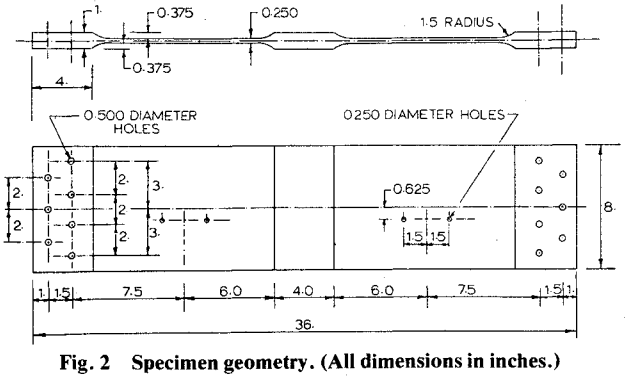

Fig. 2 Specimen geometry. (All dimensions in inches.)

Table 3 Test results

Test condition	Initial crack length (in.)	Final crack length (in.)	Flights elapsed
Spectrum A			
A1	0.038	0.108	6020.
A2	0.200	0.275	2900.
A3	0.350	0.478	3000.
A4	0.545	0.805	5000.
A5	0.091	0.141	3000.
A6	0.190	0.262	2600.
A7	0.295	0.443	5000.
Spectrum B			
B1	0.035	0.096	800.
B2	0.036	0.125	1160.
B3	0.050	0.452	2660.
B4	0.046	0.391	2460.

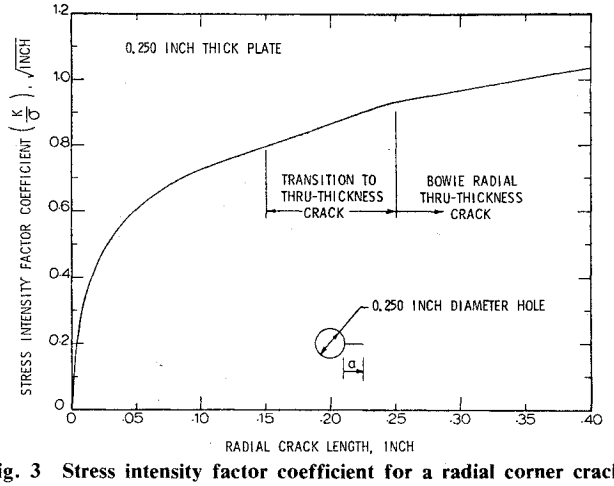

Fig. 3 Stress intensity factor coefficient for a radial corner crack emanating from a 0.250-in. hole in a 0.250-in.-thick plate.

back surface. The through-the-thickness-type crack geometry was achieved when the surface crack length, a, was approximately equal to the specimen thickness (i.e., $a=0.250$ in.). A plot of the stress intensity factor coefficient employed in this investigation is given in Fig. 3.

Crack Growth Data and Test Equipment

Crack growth was visually monitored using binocular zoom microscopes with a maximum magnification of 40X. Calibrated Mylar scales containing 0.005-in. divisions were attached to the test specimens to obtain crack length measurements. The crack lengths readings were estimated to be well within ± 0.002 in. Crack lengths were normally measured at the end of a sequence of twenty flights.

Crack growth data were collected in both dessicated air ($RH<10\%$) and laboratory air ($50<RH<80\%$). Since no discernable differences in growth rate were noted between these two environments, the growth rates were collectively used in the data base. The crack growth data collected under both constant amplitude and flight simulation loadings were reduced to obtain meaningful crack growth rate information. Fatigue crack growth rates were developed from these crack length vs applied cycles data utilizing the movable strip technique[19] using 7 consecutive data points fitted with a linear least squares determined equation (see Refs. 20 and 21 for further details).

Constant amplitude and flight simulation loads were applied using programable, closed-loop electro-hydraulic testing machines. Loads were applied in all tests at a frequency of 2.5 or 1.25 Hz. The applied loads in the load simulation tests were maintained to within 3% of programed values.

Parameters Controlling Crack Propagation

RMS Stress-to-Stress Intensity Factor

As suggested by Paris,[7] a characterizing (rms) stress parameter, which describes a stationary random process, could be employed to determine the corresponding crack tip stress intensity factor parameters through the use of

$$\bar{K}/\bar{\sigma}=K/\sigma \tag{4}$$

where (rms) parameters replace the normal deterministic stress-stress intensity factor parameters. For this investigation, the term on the right-hand side of Eq. (4) comes from Fig. 3. Paris' argument for the use of Eq. (4) was based on the fact that small crack advances do not significantly change the magnitude of the stress intensity factor coefficient function. Earlier investigators[7-11] have shown that stationary random load processes do not normally introduce significant load-interaction effects.

Cycle by Cycle Accounting Models

The three models used to calculate growth rates on a cycle by cycle basis employ the residual stress intensity factor concept. This concept suggests that the local or effective stress intensity factor (K^{eff}) at the crack tip can be calculated on a cycle-by-cycle basis using

$$K^{\text{eff}}=K^{\infty}-K_R \tag{5}$$

where K^{∞} is the stress intensity factor associated with remotely applied loads and K_R is the residual stress intensity factor which incorporates the memory of prior loading. For the linear summation cycle by cycle accounting procedure, there is no memory of prior loading so K_R is identically zero.

Residual Stress Intensity Factors

The two retardation models employed in this paper only describe the effect of decreased growth rates following an overload, so K_R in Eq. (5) is such that $K^{\text{eff}}<K^{\infty}$. The Willenborg et al.[3] retardation model develops a residual stress intensity factor (associated with an overload K^{OL}) that can be expressed in the following form[22]:

$$K_R=K_R^W=K^{OL}(1-\Delta a^{OL}/Z^{OL})-K^{\infty}_{\max} \tag{6}$$

The term Δa^{OL} represents the incremental movement of the crack subsequent to the application of the overload. The reader should note that Eq. (6) only applied when $K_R>0$; otherwise, K_R is set equal to zero (the condition for no-load interaction). The term Z^{OL} refers to the overload generated load interaction zone size which normally can be approximated by

$$Z^{OL}=(\gamma/2\pi)\ [K^{OL}/\sigma_{ys}]^2 \tag{7}$$

with a choice of $\gamma=1$ for high-strength steels[12,23] and for 2024-T3 aluminum alloy.[24-27] Other alloys, specifically Ti-6AL-4V alloy, requires that γ must be chosen larger ($\gamma\simeq 4$).[24,28]

Gallagher and Hughes[12] showed that is was possible to generalize Eq. (6) so that K_R would adequately account for the overload generated arrest boundary condition (i.e., if $(K^{OL}/K^{\infty}_{\max})\geq S$, then $da/dN=0$). The Gallagher-Hughes residual stress intensity factor is given by

$$K_R=\Phi\, K_R^W \tag{8}$$

where the proportionality factor Φ for a given remote loading is determined using

$$\Phi=[1-K_{th}/K^{\infty}_{\max}]\cdot(S-1)^{-1} \tag{9}$$

The maximum stress intensity factor (K_{th}) is associated with the fatigue crack growth threshold for a stress ratio ($R = \sigma_{min}/\sigma_{max}$) of zero.

Probst and Hillberry[25] generated fatigue crack growth data subsequent to singly applied overloads for 2024-T3 aluminum alloy and determined that crack growth arrest would occur whenever the overload ratio K^{OL}/K^{∞}_{max} was greater than a value of 2.3 (i.e., $S=2.3$). Gallagher and Hughes[12] and Petrak and Gallagher[23] assumed that S was approximately 2.3 for two different steels heat treated to various yield strength levels and found that this assumption allowed for good predictions of overload affected fatigue crack growth behavior. In this investigation, the following assumptions were made to determine the retardation parameter models identified in Eq. (7) and (9): 1) $\gamma=1$; 2) $S=2.3$; and 3) $K_{th}=2$ ksi (in.)$^{1/2}$.

Flight Crack Growth Rate Predictions

Description of Procedure

All predictions of crack growth rate are based on the procedure recently outlined by Brussat.[29] Briefly stated, the Brussat procedure develops incremental crack movements for a collection of variable amplitude loads (such as occur in a flight). These incremental crack movements are generated from various initial starting crack lengths which span the expected crack length interval for the geometry of interest. Where the crack growth rate prediction procedure employed herein differs from the Brussat approach is in the selection of the collection of variable amplitude loads. Brussat chose to employ a collection of loads which repeat with period T. Unfortunately, most spectra are presently developed with a block of many nonrepeating loads. For fighter spectra, one might have 20,000 to 50,000 load cycles in a 1000 hr flight block. Spectrum B in this investigation has approximately 105,100 load cycles in any given 300 flight mission mix block. To make the incremental crack movement approach applicable to spectra with a large period, we suggest utilizing rms parameters (or something similar) to sense the equivalency of subsets of the repeating large block of loads.

Applying Eqs. (1) and (2) to develop rms parameters based on an ordered sequence of blocks containing 50 flights ($N=N_{50}$) provides the upper and lower bounds on the parameter values identified in Table 4. Table 4 demonstrates that the influence of individual flight by flight variability can be damped out by choosing a sufficiently large group of flights. It is also noted that the 50 flight groupings provide rms parameters which compare closely with those representative of the spectrum.

The rms parameter analysis suggests that a fifty flight grouping would provide a suitable collection of variable amplitude loads typical of the spectrum. Incremental crack movements were therefore generated using all the loads in a fifty flight block; the equation describing the calculation method is:

$$\Delta a = a_f - a_o = \sum_{i=1}^{N_{50}} \left.\frac{da}{dN}\right|_i \tag{10}$$

i.e., the fatigue crack growth rate for each applied load cycle in a block of 50 flights was summed. Additional details on how the fatigue crack growth rates are calculated can be found below. By repeatedly increasing the initial crack length (a_o) by a factor of 1.3, an initial crack length range of 0.035 to 0.627 was covered for twelve incremental crack movements. To obtain the average growth rate per flight, the incremental crack movements defined by Eq. (10) were divided by the number of applied flights (50) used in generating the increment.

Rather than selecting any specific 50 flight grouping of loads when using the cycle by cycle analysis, 12 consecutive 50 flight groups were taken from the first 600 flights applied in each of the two spectra considered. For the cycle by cycle analysis, the first incremental crack movement was obtained using Eq. (10) wherein the individual growth rates were associated with the first 50 flights in a spectrum, the second movement (from a new a_o) was associated with flights 51 to 100, and so forth until 12 growth increments were generated. For the stress-stress intensity factor characterization approach, the representative flight repeats throughout the spectrum so in applying Eq. (10), the representative flight is repeated 50 times.

Table 4 Upper and lower bounds on rms stress parameters[a]

Parameter	Spectrum	Lower bound	Upper bound
$\bar{\sigma}_{max}$ (ksi)	A	11.72	11.74
	B	11.97	12.55
$\overline{\Delta\sigma}$ (ksi)	A	5.98	6.23
	B	4.38	4.49
$\bar{\sigma}^{\rho}_{max}$ (ksi)	A	13.38	13.61
	B	17.87	18.97
$\bar{\sigma}^{\rho}_{min}$ (ksi)	A	−15.57	−14.95
	B	−15.19	−14.89
$<N_F>$	A	31	31
	B	337	367

[a] Based on 120 consecutive 50-flight groupings in spectra.

Determining the Cyclic Crack Growth Rate

In the application of Eq. (10), a continuous update of crack length is employed as the crack moves from its initial position a_o prior to the calculation of stress intensity factors and hence cyclic crack growth rates $[\,(da/dN)|_i\,]$. The cyclic crack growth rate is obtained for each load application employing a stress intensity factor-crack growth rate relationship of the following form:

$$\left.\frac{da}{dN}\right|_i = f(K_{max}, R) \tag{11}$$

where the choice of K_{max} and R is dictated by the method of calculating the controlling stress intensity factor. For the cycle by cycle accounting approaches, Eq. (5) is evaluated using the maximum load in a given load cycle to obtain $K_{max}=K^{eff}_{max}$ and the stress ratio R in Eq. (11) is obtained from

$$R = R^{eff} = (K^{\infty}_{min} - K_R)/(K^{\infty}_{max} - K_R) \tag{12}$$

where $K_R=0$, or K_R is calculated using Eqs. (6) or (8). When the rms parameter approaches were used, the cyclic crack growth rate is determined using the spectrum's representative rms maximum stress intensity factor and rms stress ratio applied on a per cycle basis.

The functional form of the stress intensity factor-crack growth relationship is given by the following two equations:

$$f(K_{max}, R<0) = 8.133\times10^{-8}(K_{max})^{2.150} \tag{13}$$

and

$$f(K_{max}, R\geq 0) = 8.631\times10^{-8}\,[\,[K_{max} - 3(1-R)^{-0.35}]\,(1-R)^{0.696}\,]^{2.347} \tag{14}$$

Equations (13) and (14) were found to describe the constant amplitude crack growth rate data that were collected in conjunction with the flight by flight test program. Stress ratios of −1, −0.83, 0.1, 0.2, 0.4, 0.5, and 0.67 were used in this constant amplitude test program. The negative stress ratio equation [Eq. (13)] was based on crack growth rate data between 5 and 200 μ in./cycle, while the positive stress ratio equation [Eq. (14)] was developed using crack growth rates between 0.1 and 200-μ in./cycle.

Results and Discussion

Flight Simulation Crack Growth Rates

Figure 4 describes the crack growth rate behavior generated under loading by spectra A and B for the crack length increments given in Table 3. The crack growth rate data are portrayed as a function of the rms maximum stress intensity factor which was calculated using the representative rms maximum stresses given in Table 1 and Eq. (4) evaluated with the stress intensity factor coefficient presented in Fig. 3. Identified in Fig. 4 are least-squares determined power law curves of the type

$$da/dF = C(\bar{K}_{max})^p \qquad (15)$$

that were developed to describe the general and mean trend of the data.

In the following subsections, comparisons will be made between the fitted curves shown in Fig. 4 and predictions which were determined utilizing both cycle by cycle accounting procedures and rms stress-stress intensity factor characterization approaches. The average growth per flight determined by any of the predictive procedures to be discussed is always portrayed as a function of the rms maximum stress intensity factor evaluated at the center of the growth increment given by Eq. (10) (i.e., at $(a_o+a_f)/2$] using Fig. 3 and the representative rms maximum stresses given in Table 1. This procedure was followed so that predictions can be directly compared with the flight simulation generated crack growth rate data.

Cycle by Cycle Analyses

Shown in Fig. 5 are the predictions based on the cycle by cycle accounting procedures. Each individual point shown was obtained using the crack incrementation scheme described by Eq. (10) and its supporting discussion. Figure 5 shows that the trend established by the cycle-by-cycle predictions closely follows those established by the two data sets. Figure 5 indicates that the no-load-interaction, linear summation procedure produces growth rate predictions that are slightly faster than the data trend for the upper surface spectrum (A) and approximately a factor of two times faster for the lower surface spectrum (B). These predictions support the earlier conclusions of Brussat[1] who suggested that linear summation predictions provide a conservative upper bound on spectrum crack growth data.

As shown in Fig. 5, the application of both retardation models produced growth rate predictions that are lower than those generated using the no-load-interactions, linear summation approach. The growth rates associated with both retardation models provide a reasonable description of the magnitude and trend of the data generated by Spectrum A while the Gallagher-Hughes model provides the better fit for the crack growth behavior generated by Spectrum B. The additional retardation associated with the Willenborg et al. model results in nonconservative predictions for the lower growth rate region of the Spectrum B data.

Stress-Stress Intensity Factor Characterization

Shown in Fig. 6 are the predictions based on two rms stress spectrum characterization approaches. The first rms characterization approach reduces the load sequences from that typically described by Fig. 1 to a block of constant amplitude cycles for an average flight which has the stress levels defined by Table 1. The second approach assumes that the peak to peak (minimum to maximum) stress level in a given flight controls the crack growth induced by the flight and thereby reduces the 6000 flight spectra to 6000 constant amplitude cycles having the stress levels identified in Table 2 for any given flight. In both cases, the corresponding rms stress intensity factors are evaluated using the quantities identified in Tables 1 and 2 and the stress intensity factor coefficient given in Fig. 3 via Eq. (4).

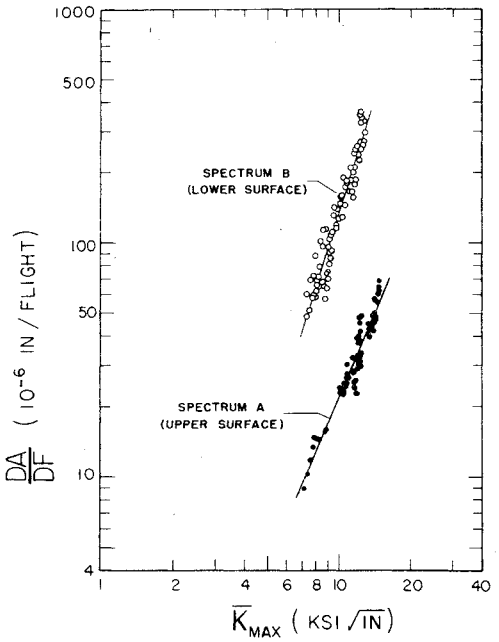

Fig. 4 Flight simulation crack growth rates as a function of the rms maximum stress intensity factor.

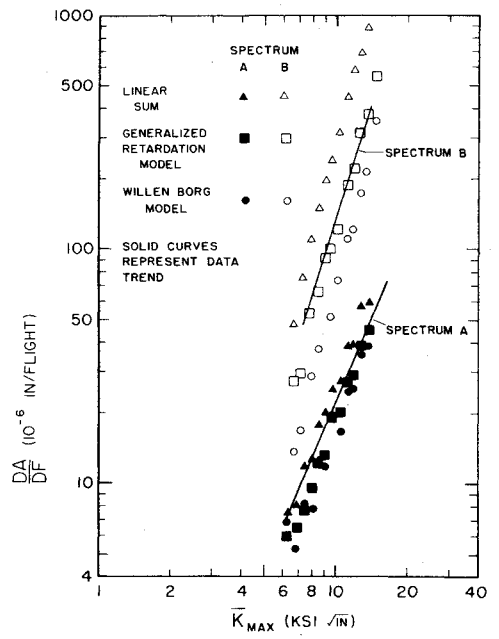

Fig. 5 Cycle-by-cycle predictions of flight simulation crack growth rate trends.

The predictions based on the Table 1 rms stress characterization are shown by Fig. 6 to lead to crack growth rates that are overly conservative especially in the high growth rate region. As can be seen by the figure these rms predictions follow a trend that diverges from the data established trend, a pattern that is similar to that reported by Smith.[8] Smith noted this divergence between crack growth rate data generated under random stress histories which had a constant mean stress and a continuous (Rayleight) distribution of stress ranges. In Fig. 6, the magnitude of the divergence of the rms established curve from that established by the data appears to be substantially greater than that observed by Smith.

The choice of the second rms stress characterization approach was dictated by a desire to isolate the large amplitude stresses and to determine their effect on growth independent of the small amplitude, high stress ratio cycles that normally occur in transport wing stress spectra. Using Eq. (10), and repeating the once-per-flight, peak-to-peak stress (from

Table 5 Life prediction ratios

Test condition \ Model	Least square fit	Linear summation	Generalized retardation	Willenborg retardation	rms all stresses	Peak-to-peak stresses
Spectrum A						
A1	0.90	0.94	1.28	1.36	0.54	1.31
A2	0.93	0.82	1.13	1.28	0.31	1.43
A3	1.15	0.93	1.29	1.50	0.30	1.78
A4	1.01	0.76	1.06	1.26	0.20	1.59
A5	1.12	0.93	1.26	1.38	0.44	1.41
A6	1.11	0.91	1.26	1.42	0.35	1.58
A7	0.90	0.70	0.97	1.12	0.23	1.31
Spectrum B						
B1	1.27	0.75	1.59	2.94	0.75	4.65
B2	1.10	0.63	1.35	2.48	0.63	4.24
B3	0.95	0.47	1.03	1.83	0.46	4.78
B4	0.98	0.50	1.09	1.93	0.49	4.76

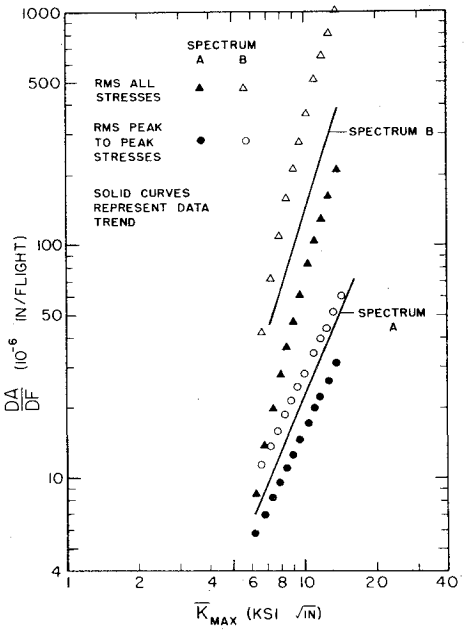

Fig. 6 Root mean square stress-stress intensity factor predictions of flight simulation crack growth rate trends.

Table 2) 50 times would be equivalent to the application of 50 flights of variable amplitude loading if all the fatigue growth damage results from the application of this major cycle.

As can be noted from Fig. 6, the peak-to-peak predictions closely follow the data-established least-squares curve for Spectrum A which implies that the once-per-flight, peak-to-peak stress is the major contributor of fatigue damage in this spectrum. Figure 6 shows that the once-per-flight, peak-to-peak stress contributes less than half the fatigue damage in Spectrum B as indicated by the difference between the predictions and the data established curve.

Overall Evaluation of Approaches Considered

As an alternative to comparing the magnitude and trend of the predicted crack growth rates to that of the data, one could compare the ability of the predictive approaches to predict the crack-length vs flight behavior, that which was derived directly by test. By fitting curves of the type described by Eq. (15) to the predicted crack growth rate data points, estimates can be obtained for the number of elapsed flights required to move the crack from its initial to final lengths using

$$F_{\text{pred}} = \sum_{i=1}^{n-1} \Delta F_i = \sum_{i=1}^{n-1} \left[\frac{a_{i+1} - a_i}{C(\bar{K}_{\max})^{n_i}} \right] \qquad (16)$$

The quantities a_i and a_{i+1} are any two consecutive crack length data points from a set of n points. Table 5 lists the life prediction ratios, the predicted to actual flights elapsed ratio, for each of the predictive approaches as applied to the crack length, elapsed flight data identified in Table 3. Also included in Table 5 are the life prediction ratios based on the least squares determined fit to the data shown in Fig. 4. Note that life prediction ratios less than one (1.0) are conservative.

Table 5 shows that a least squares determined curve based on derived flight by flight growth rates will, when integrated, successfully reconstruct the original data on which it was based, not too surprisingly. The cycle-by-cycle load interaction accounting procedures provided the best correlation for predicting the trends of the growth rate data as exhibited by Fig. 5. The different magnitudes of the cycle-by-cycle growth rate predictions consistently result in conservative, slightly nonconservative, and nonconservative life prediction ratios for the linear summation, the generalized retardation model, and the Willenborg retardation model, respectively. Recall that the generalized retardation model as described by Eqs. (6-9) was developed using as a boundary condition the overload ratio that produced no growth subsequent to an overload. Some recent experimental evidence developed by Hillberry and coworkers[30] on 2024-T3 Aluminum would suggest that when tensile overloads are followed by compressive underloads the value of the overload shutoff ratio (S) should be greater than 2.3, the value assumed herein. Assuming values of S greater than 2.3 for the generalized retardation model produces predictions which are more conservative than those shown in Fig. 5 and listed in Table 5. Additional studies will be needed to document the correct choice of the overload shutoff ratio for use with this model.

The two rms stress-stress intensity factor characterization approaches are shown by Fig. 6 and Table 5 to result in overly conservative predictions for the approach based on the Table 1 spectrum characterization and in nonconservative predictions based on the once-per-flight, peak to peak stress (Table 2) spectrum characterization. While utilizing rms stress characterizations of the stress spectrum are desirable from a computational time point of view, the results of this evaluation indicate that these rms parameters do not properly characterize the transport wing stress history, thereby resulting in predictions which are not accurate either for determining the magnitude or trend of the data. One consequence of the rms approach is that it results in equalizing the effects of small and large stresses (maxima and ranges) to an average. The small stresses essentially become more effective while the large stresses are made less effective.

The crack growth rate (da/dF) vs a characterizing stress intensity factor ($\bar{K}_{\max}$) format such as presented in Fig.4 represents a simple and useful approach for directly evaluating flight-loading-induced crack-growth behavior.

Such a format is suggested for comparing crack growth behavior when experimental studies of either stress effects (such as magnitude scaling, high-stress-level clipping, or low-stress-level truncation) or mission sequence effects are being conducted. These types of effects are easily evaluated by comparison with the magnitude and trend of the curve established by the baseline condition. A word of caution must be added before curves of the type suggested by Eq. (15) are applied to predicting the crack growth behavior of other structural geometries (including crack geometries) which differ appreciably from that chosen for the data collection. For flight-induced crack-growth behavior, Schijve et al.[31] have noted that attention must be given to the rate of change in the stress intensity factor with crack length, i.e., dK/da. Since each structural geometry has a unique stress intensity derivative, Eq. (15) evaluated for one structural geometry might not provide the transfer function needed to predict the crack growth behavior associated with a significantly different structural geometry. This transfer function topic needs further work.

Conclusions

Based on the information presented in this paper, the following conclusions appear reasonable and pertinent to the charcterization of crack growth data generated with transport-wing flight-simulation stress histories. 1) Unimodal stress distributions do not characterize these spectra such that a single set of rms stress parameters ($\bar{\sigma}_{max}$, $\bar{\Delta\sigma}$) would be useful for accurately determining flight by flight cracking rates. 2) No-load interaction, linear summation, and cycle-by-cycle accounting procedures can provide an upper (conservative) bound to crack growth rate behavior. 3) By incorporating the generalized high-to-low load interaction model discussed herein into a cycle by cycle accounting procedure, close estimates of both the trend and magnitude (i.e., mean) of crack growth rate data result. 4) Integration of predictive crack growth trend lines provides direct verification of the usefulness of approach described in this paper.

References

[1] Brussat, T. R., "An Approach to Predicting the Growth to Failure of Fatigue Cracks Subjected to Arbitrary Uniaxial Cyclic Loading," *Damage Tolerance in Aircraft Structures,* ASTM STP 486, 1971, American Society For Testing and Materials, Philadelphia, Pa., pp. 122-143.

[2] Wheeler, O.E., "Spectrum Loading and Crack Growth, *Transactions of the ASME, Series D:* Vol. 94, March 1972, p. 181.

[3] Willenborg, J. D., Jr., Engle, R. M., and Wood, H. A., "A Crack Growth Retardation Model Using an Effective Stress Concept," AFFDL-TM-71-1-FBR, Jan. 1971, Air Force Flight Dynamics, Lab., Wright-Patterson Air Force Base, Ohio.

[4] Paris, P. C., Bucci, R. J., Cotter, K. H., and Schmidt, D., "Analytical Methods and Improved Instrumentation for Crack Closure Effects in Variable Amplitude Fatigue Crack Growth," presented at the Seventh National Symposium on Fracture Mechanics, College Park, Md., Aug. 1973.

[5] Wood, H. A.,"A Summary of Crack Growth Prediction Techniques," *Fatigue Life Prediction for Aircraft Structures and Materials,* Chap. 8, AGARD LS 62, May 1973, Advisory Group for Aerospace Research and Development, NATO.

[6] Porter, T. R., "Method of Analysis and Prediction for Variable Amplitude Fatigue Crack Growth," *Journal of Engineering Fracture Mechanics,* Vol. 4, 1972, pp. 717-736.

[7] Paris, P. C., "The Fracture Mechanics Approach to Fatigue," *Fatigue, An Interdisciplinary Approach,* edited by J. J. Burke, N. L. Reed, and V. Weiss, Syracuse Univ. Press, Syracuse, N.Y., 1964, pp. 107-132.

[8] Smith, S. H., "Fatigue Crack Growth Under Axial Narrow and Broad Band Random Loading," *Acoustical Fatigue in Aerospace Structures,* edited by W. J. Trapp and D. M. Forney, Syracuse Univ. Press, Syracuse, N. Y., 1965, pp. 331-360.

[9] Smith, S. H., "Random-Loading Fatigue Crack Growth Behavior of Some Aluminum and Titanium Alloys," *Structural Fatigue in Aircraft,* ASTM STP 404, 1966, American Society for Testing and Materials, Philadelphia, Pa, pp.74-100.

[10] Swanson, S. R., Cicci, F., and Hoppe, W., "Crack Propagation in Clad 7079-T6 Aluminum Alloy Sheet Under Constant and Random Amplitude Fatigue Loading," *Fatigue Crack Propagation,* ASTM STP 415, 1967, American Society for Testing and Materials, Philadelphia, Pa., pp. 312-362.

[11] Barsom, J. M., "Fatigue-Crack Growth Under Variable Amplitude Loading in ASTM A 514B Steel," *Progress in Flaw Growth and Fracture Toughness Testing,* ASTM STP 536, 1973, American Society for Testing and Materials, Philadelphia, Pa., pp. 147-167.

[12] Gallagher, J. P. and Hughes, T. F., "Influence of Yield Strength on Overload Affected Fatigue Crack Growth Behavior in 4340 Steel," AFFDL-TR-74-27, July 1974, Air Force Flight Dynamics Lab., Wright Patterson Air Force Base, Ohio.

[13] Sayer, R. B., "Nonlinear Effects of Spectrum Loading on Fatigue Crack Growth in Transport Wings," AIAA Paper 74-984, Los Angeles, Calif., 1974.

[14] McMillan, J. C., and Pelloux, R. M. N., "Fatigue Crack Propagation Under Program and Random Loads," *Fatigue Crack Propagation,* ASTM STP 415, 1967, American Society for Testing and Materials, Philadelphia, Pa., pp. 505-535.

[15] Barsom, J. M., "Effect of Cyclic Stress Form on Corrosion Fatigue Crack Propagation Below K_{Iscc} in a High Yield Strength Steel," *Corrosion Fatigue: Chemistry, Mechanics, and Microstructure,* edited by O.F. Devereux, A. J. McEvily, and R. W. Staehle, National Association of Corrosion Engineers, 1972, Houston, Tex. pp. 424-435.

[16] Walker, E. K., "The Effect of Stress Ratio During Crack Propagation and Fatigue for 2024-T3 and 7075-T6 Aluminum," *Effects of Environment and Complex Load History on Fatigue Life,* ASTM STP 462, 1970, American Society of Testing and Materials, Philadelphia, Pa., pp. 1-14.

[17] Forman, R. G., Kearney, V. E., and Engle, R. M., "Numerical Analysis of Crack Propagation in Cyclically Loaded Structures," *Transactions of the ASME, Series D, Journal of Basic Engineering,* Vol. 89, Sept. 1967, pp. 459-464.

[18] Hsu, T. M. and Lui, A. F., "Stress Intensity Factors for Truncated Elliptical Cracks," presented at the Seventh National Symposium on Fracture Mechanics, College Park, Md., Aug. 1973.

[19] Gallagher, J. P. "Experimentally Determined Stress Intensity Factors for Several Contoured Double Cantilever Beam Specimens," *Journal of Engineering Fracture Mechanics,* Vol. 3, 1971, pp. 27-43.

[20] Clark, W. G. and Hudak, S. J., "Variability in Fatigue Crack Growth Rate Testing," ASTM E-24.04.01 Task Group Rept., Sept. 1974, American Society for Testing and Materials, Philadelphia, Pa.

[21] Gallagher, J. P., Martin, J., Coffin, S., and Stalnaker, H. D., "Using the Movable Strip Technique to Generate Crack Growth Rates," AFFDL-TR-75-XXX, Air Force Flight Dynamics Lab., Wright Patterson Air Force Base, Ohio, (in preparation).

[22] Gallagher, J. P., "A Generalized Development of Yield Zone Models, "AFFDL-TM-74-28-FBR, Jan. 1974, Air Force Flight Dynamics Lab., Wright Patterson Air Force Base, Ohio.

[23] Petrak, G. J. and Gallagher, J. P., "Predictions of the Effect of Yield Strength on Fatigue Crack Growth Retardation in HP 9Ni-4Co-30C Steel," *Transactions of the ASME, Journal of Engineering Materials and Technology,* Vol. 97, Series H, July 1975, pp.206-213.

[24] Gray, T. D., "Fatigue Crack Retardation Following a Single Overload," AFFDL-TM-73-137-FBR, Oct. 1973, Air Force Flight Dynamics Lab., Wright Patterson Air Force Base, Ohio.

[25] Probst, E. P. and Hillberry, B. M., "Fatigue Crack Delay and Arrest Due to Single Peak Tensile Overloads," *AIAA Journal,* Vol. 12, March 1974, pp. 330-335.

[26] Von Euw, E. F. J., Hertzberg, R. W., and Roberts, R., "Delay Effects in Fatigue Crack Propagation," *Stress Analysis and Growth of Cracks,* ASTM STP 513, 1972, American Society for Testing and Materials, Philadelphia, Pa., pp. 230-259.

[27] Trebules, V. W., Jr., Roberts, R., and Hertzberg, R. W., "Effect of Multiple Overloads on Fatigue Crack Propagation in 2024-T3 Aluminum Alloy," *Progress in Flaw Growth and Fracture Toughness Testing,* ASTM STP 536, 1973, American Society for Testing and Materials, Philadelphia, Pa., pp. 115-146.

[28] Wei, R. P., Shih, T. H., and Fitzgerald, H. J., "Load Interaction Effects on Fatigue Crack Growth in Ti-6A1-4V Alloy," CR-2239, April 1973, NASA.

[29] Brussat, T. R., "Rapid Calculation of Fatigue Crack Growth by Integration," *Fracture Toughness and Slow-Stable Cracking,* ASTM STP 559, 1974, American Society for Testing and Materials, Philadelphia, Pa., pp. 298-311.

[30] Hillberry, B. M., Purdue University, private communication, Oct. 18, 1974.

[31] Schijve, J., Jacobs, F. A., and Tromp, P. J., "Fatigue Crack Growth in Aluminum Alloy Sheet Material Under Flight-Simulation Loading. Effects of Design Stress Level and Loading Frequency," NLR TR 72918U, Feb. 1972, National Aerospace Laboratory (NLR), Amsterdam, The Netherlands.